Regular Paper
J. Korean Inst. Electr. Electron. Mater. Eng.
Vol. 31, No. 5, pp. 300-306 July 2018
DOI: https://doi.org/10.4313/JKEM.2018.31.5.300
ISSN 1226-7945(Print), 2288-3258(Online)

막대형 Ni-Zn 페라이트 입자의 합성 및 특성 평가

전승엽, 황진아, 전명표[a]
한국세라믹기술원

Synthesis and Characterization of Rod-Shaped Ni-Zn Ferrite Particles

Seung-Yeop Chun, Jin-Ah Hwang, and Myoung-Pyo Chun[a]
Korea Institute of Ceramic Engineering and Technology, Jinju 52851, Korea

(Received December 12, 2017; Revised March 13, 2018; Accepted March 20, 2018)

Abstract: The rod-shaped $Ni_{0.5}Zn_{0.5}Fe_2O_4$ particles were synthesized via a topotactic reaction, in which goethite (α-FeOOH) particles are the main constituents. The phases, microstructures and magnetic properties of these particles were studied using XRD, FE-SEM and VSM. The precursor solution consisted of $NiSO_4 \cdot xH_2O$, $ZnSO_4 \cdot xH_2O$, goethite and D.I. water werereacted at four different temperatures (50, 70, 90, 100℃) to generate four differently precipitated particles respectively. During the co-precipitation reaction, the pH of the solution was maintained at 8.0 using NaOH. The particles co-precipitated and calcined at a temperature of 700℃, exhibited a rod-shape similar to its original goethite, which means that the shape of Ni-Zn ferrite particles can be topotactically controlled by the goethite. The particles synthesized at 70 and 90℃ have a saturation magnetization of 29 and 35 emu/g respectively; representing better values than the ones synthesized at the 50 and 100℃, in which some second phases such as Fe_2O_3 were observed.

Keywords: Ni-Zn ferrite, Rod shape, Topotactic, Goethite, Precursor solution, Magnetic

1. INTRODUCTION

Since Ni-Zn ferrite has a relatively high magnetic permeability and low loss in the wide frequency range, it has been extensively used in many applications such as inductor, transformer, and wireless power charger, etc. Ni-Zn ferrite particles have been fabricated using many methods such as electro-deposition, sol‐gel, solid state raction, chemical co-precipitation, hydrothermal synthesis, combustion reaction, mechano-chemical, citrate precursor techniques, and micro-emulsion [1-9]. However, there are few studies about a synthesis of rod shaped Ni-Zn ferrite particles which is expected to enhance the magnetic shape anisotropy contributing to increasing magnetic permeability due to their one dimensional structure.

In this paper, rod-shaped Ni-Zn ferrite particles were synthesized through a topotactic reaction method using goethite (α-FeOOH) particles as topotactic source materials. Ni and Zn sulfide anhydros such as $NiSO_4 \cdot xH_2O$ and $ZnSO_4 \cdot xH_2O$ were used as Ni and Zn sources, respectively. Source reagents composed of goethite, Ni and Zn sulfide anhydrous were mixed in D.I. water and reacted at four different temperatures (50, 70, 90 and 100℃) in order to determine the optimum temperature because reaction temperature is related to the reaction rate of the source materials which can affect on the magnetic properties of the synthesized particles.

a. Corresponding author; myoungpyo@kicet.re.kr

2. METHOD FOR EXPERIMENT

The rod-like $Ni_{0.5}Zn_{0.5}Fe_2O_4$ particles were synthesized through the two step process, where the first one is to synthesize goethite (α-FeOOH) particles and the next one is to fabricate Ni-Zn ferrite particles by topotatic reaction using goethite particles already prepared as a major source material.

2.1 Synthesis of goethite

The $FeSO_4 \cdot 7H_2O$ (Sigma Aldrich) used as the Fe-source was dissolved in distilled water in three necked flask by stirring for 30 minutes. On the purpose of removing the effect of oxygen on the synthesis process, the process was conducted in N_2 atmosphere with supplying N_2 gas into the flask and with draining it outside at the same time. The precursor solution was adjusted to pH = 8.0 by dripping NaOH into the reaction flask and then reacted for 2 hours. The concentration ratio of the reactants, R $[(OH)^-/Fe(II)^{2+}]$, is one of the most important factors in determining the quality of the synthesized particles and was fixed at 4.5.

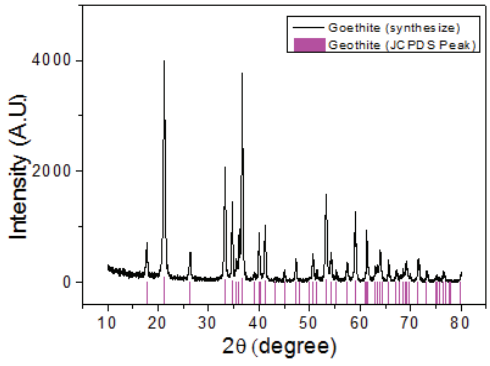

Fig. 1. X-ray diffraction pattern of synthesized goethite powder.

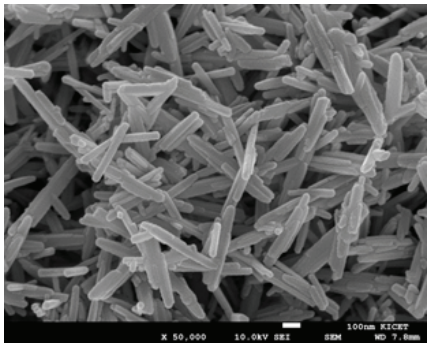

Fig. 2. FE-SEM image of synthesized goethite powder.

When the precursor solution completely turns blue from colorless in the course of the reaction, it means that the reaction proceeds well and that intermediate phase $Fe(OH)_2$ is formed. The goethite particles were synthesized by further reacting a blue suspension of $Fe(OH)_2$ at 50℃ for 6 hours. During this time, air should be continuously supplied to the flask. The synthesized goethite particle was analyzed using an X-ray diffraction (XRD, D/max Rigaku 2,200 V/PC). Its microstructure was observed with field emission scanning electron microscopy (FE-SEM, JSM-6700F). Figure 1 shows the X-ray diffraction (XRD) pattern of synthesized goethite particles and the peak position of the measured XRD pattern matches exactly one-to-one with pure goethite JCPDS pattern. Figure 2 is the FE-SEM image of synthesized goethite particles and clearly shows uniformly rod-shaped particles of 70 to 80 nm in diameter and 400 nm in length.

2.2 Synthesis of Ni – Zn ferrite

The rod-shaped Ni-Zn ferrite particles were synthesized through a topotactic reaction method using goethite particles as topotactic source materials. Ni and Zn sulfide anhydrous such as $NiSO_4 \cdot 6H_2O$ and $ZnSO_4 \cdot 7H_2O$ were used as Ni and Zn sources, respectively. Source reagents composed of goethite, Ni and Zn sulfide anhydros were mixed in D.I. water and reacted at four different temperatures (50, 70, 90, and 100℃) in order to determine the optimum temperature.

Figure 3 is a schematic diagram for synthesizing Ni-Zn ferrite. At first, 1 mole of $NiSO_4 \cdot 6H_2O$ and 1 mole of $ZnSO_4 \cdot 7H_2O$ are placed in a three-necked flask containing 300 ml of distilled water and sufficiently dissolved at 50℃. Subsequently, a goethite solution dispersed in 300 ml of distilled water is added to the flask and a reaction is carried out at four different reaction temperatures of 50, 70, 90, and 100℃, respectively. 3 mol Na_2CO_3 aqueous solution is slowly added dropwise to adjust the pH of the precursor

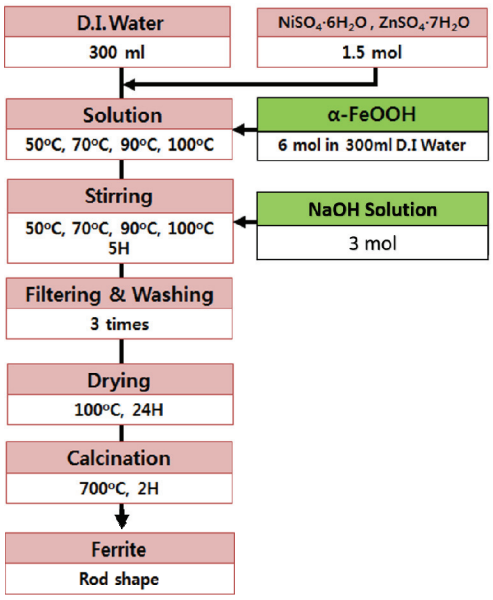

Fig. 3. Schematic diagram for synthesized rod-shaped Ni-Zn ferrite particles.

solution to 8.0.

As the reaction progresses, the starting materials, $NiSO_4 \cdot 6H_2O$ and $ZnSO_4 \cdot 7H_2O$ coprecipate with goethite in the form of hydroxides such as NaOH · $Zn(OH)_2$ and $Ni(OH)_2$, respectively, on the bottom of the flask as shown in the following equations (1)~(3).

$$Na_2CO_3 + H_2O \rightarrow 2NaOH + CO_2 \quad (1)$$

$$ZnSO_4 + 2NaOH \rightarrow Zn(OH)_2 + Na_2SO_4 \quad (2)$$

$$NiSO_4 + 2NaOH \rightarrow Ni(OH)_2 + Na_2SO_4 \quad (3)$$

$$Zn(OH)_2 \rightarrow H_2O + ZnO \quad (4)$$

$$Ni(OH)_2 \rightarrow H_2O + NiO \quad (5)$$

$$2FeOOH \rightarrow Fe_2O_3 + H_2O \quad (6)$$

After the co-precipitation reaction is completed, the precipitate is washed with ethanol and then centrifuged at 2,000 rpm for 10 minutes. These washing and filtering step are carried out three times. Synthetic Intermediates such as Na_2SO_4, which is completely dissolved in distilled water in the form of a colorless aqueous solution, are almost eliminated during washing and centrifugation. The refined precipitate dried in an oven at 100℃ for 24 hours is crushed and calcined at 700℃ for 2 hours in air to synthesize a rod shaped Ni-Zn ferrite powder. The hydroxides such as $Zn(OH)_2$ and $Ni(OH)_2$ constituting the precipitate will be dehydrated by the reaction of the equations (4), (5) to become ZnO and NiO, respectively and these ZnO and NiO will react with the goethite to create the rod shape Zn ferrite powder.

The synthesized rod-like Ni-Zn ferrite powder was analyzed using an XRD Its microstructure was observed with FE-SEM and magnetic properties such as permeability and saturation magnetization were investigated by material analyzer and vibrational standing magnetometer (VSM, Molspin VSMNUVO), respectively.

3. RESULTS AND DISCUSSIONS

3.1 Structural analysis

Figures 4(a) and (b) show the X-ray diffraction pattern and the enlarged diffraction lines (311) of the powder calcined at 700℃ after co-precipitation at 50, 70, 90 and 100℃. Powders co-precipitated at 70 and 90℃ correspond to the spinel structure (JCPDS 10-0325) [10] but powders co-precipitated at 50 and 100℃ show many weak diffraction peaks identified as a secondary phase of α-Fe_2O_3 besides the ferrite phase [11]. It should be noticed that the intensity of α-Fe_2O_3 is further increased at 100℃ as shown in Fig. 4. Goethite (α-FeOOH) alone is generally decomposed into Fe_2O_3 as shown in equation (6). Therefore, it seems like that a part of goethite surface did not co-precipitate along with $Zn(OH)_2$ and $Ni(OH)_2$ at 50 and 100℃ and resulted in Fe_2O_3. Such a behavior can be attributed to a restricted co-precipitation reaction among goethite, $Zn(OH)_2$ and $Ni(OH)_2$ due to a high thermal agitation at 100℃ as well as an insufficient co-precipitation reaction at 50℃. Harali, *et al.* reported that hematite (α-Fe_2O_3) appears during the synthesis of NiCuZn ferrite particles when the co-precipitation reaction time is not enough [12].

Figure 5 shows the dependence of the lattice parameter

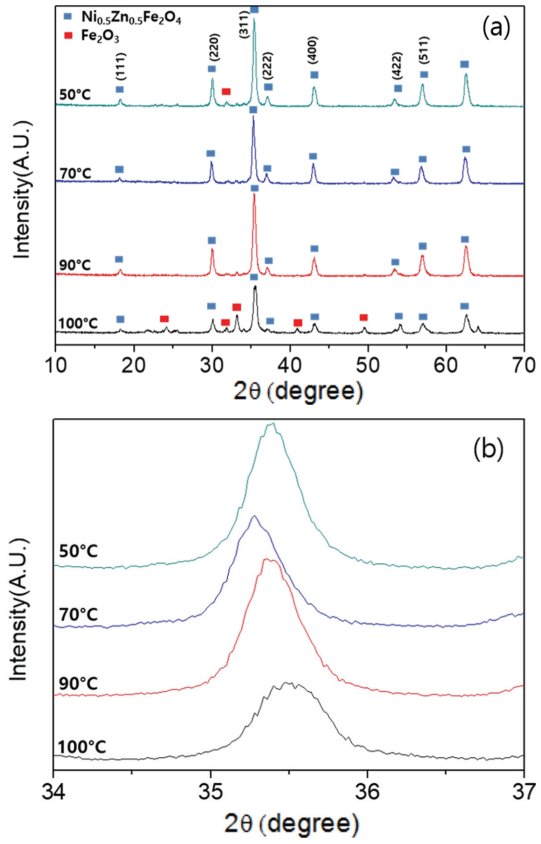

Fig. 4. (a) X-ray diffraction patterns of $Ni_{0.5}Zn_{0.5}Fe_2O_4$ powders synthesized at various temperatures and followed by calcination at 700℃ and (b) enlarged diffraction lines (311).

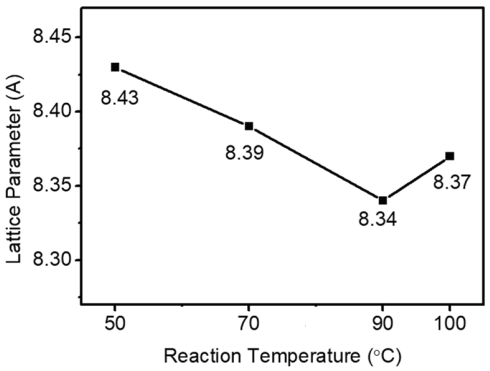

Fig. 5. Lattice parameter of $Ni_{0.5}Zn_{0.5}Fe_2O_4$ powders synthesized at various temperatures and followed by calcination at 700℃.

of the ferrite powder on the co-precipitation reaction temperature. The lattice parameter was calculated by the least squares method using diffraction lines (311), (220), (400) and (440). As the co-precipitation temperature increases from 50℃ to 100℃, the lattice parameter monotonically decreases from 8.43 Å to 8.34 Å in the temperature range of 50℃ to 100℃, showing the lowest value at 90℃ but after that goes up to 8.3641 Å at 100℃. The lattice parameters of the synthesized $Ni_{0.5}Zn_{0.5}Fe_2O_4$ ferrite nanoparticles closely match those published in JCPDS-47-0023.

In the spinel ferrite, it is well known that Zn^{2+} ions prefer to occupy the tetrahedral A-sites and Ni^{2+} ions prefer to occupy the octahedral B-site whereas Fe^{3+} ions partially occupy the A-sites and the B-sites [13]. The lattice parameters of the Ni-Zn ferrite particles depend on the preparation method, the phase composition and in particular is very sensitive to the concentration ratio between Ni and Zn ions. many reports [14-16] have been made that the lattice parameter of Ni-Zn ferrite is montonically decreased as increasing the Ni^{2+} ions. That is reason considering the smaller ionic radius of Ni^{2+} ion (0.69 Å) as compared to the ionic radius of Zn^{2+} ion (0.74 Å) and is similar to the decreasing tendency of the lattice parameter of our Ni-Zn ferrite powder according to the co-precipitation reaction temperature. Therefore, it is considered that the relative concentration of Ni ions to Zn ions in the synthesized Ni-Zn powders is constantly increased in the reaction temperature of 50 to 90℃ and decreased over this temperture range. More $Ni(OH)_2$ than $Zn(OH)_2$ can be made during the reaction process to create the Ni-rich and rod like Ni-Zn ferrite particles co-precipitating with the goethite particles because the solubility of Ni ion in aqueous solution is stronger than that of Zn [17].

3.2 Morphology and crystallite size

The size of the crystallite was calculated by the Debye-Scherrer's method of equation (7) using the diffraction line (311) shown in Fig. 4(b) [18].

$$D = k\lambda / B\cos\theta \quad (7)$$

Where D is the average crystallite size, k is the Scherrer constant (0.89), λ is the wave length of X-ray beam used, B is the full-with at half maximum

(FWHM) of diffraction peak and θ is the Bragg's angle of the diffraction line (311).

Figure 6 shows the particle size of the calcined powders at 700℃ after co-precipitation at 50, 70, 90, and 100℃, respectively. As the co-precipitation reaction temperature increases from 50℃ to 100℃, the particle size of the Ni-Zn ferrite gradually increases from 20 nm to 58 nm as shown in Fig. 6, which is similar to the dependence of the particle size on the Ni ion concentration. The average particle size increase with increase of Ni ion concentration was reported in the literatures [19].

Figure 7 shows FE-SEM images of Ni-Zn ferrite powders calcined at 70℃ after co-precipit ation at four reaction temperatures. The synthesized Ni-Zn ferrites have rod-like particles, similar to the goethite irrespective of the reaction temperature. It should be noticed that many small debris particles are also observed in the Ni-Zn powders synthesized at 50℃ and the number of these particles monotonically decreases until the co- precipitation temperature reaches 90℃, therefore, which seems attributed to the insufficient and non-uniform co-precipitation of the reagents containing goethite at the low temperature. Ferrite powder synthesized at 70℃ have the fewest debris particles and the shape of the rod is well shown in it.

The ferrite powder synthesized at 100℃ has much more debris particles than that at 70℃ and also shows agglomeration, which likely to be because some goethite particles that can not precipitate together with $Zn(OH)_2$ and $Ni(OH)_2$ are precipitated singly and converted to hematite (Fe_2O_3) during calcination.

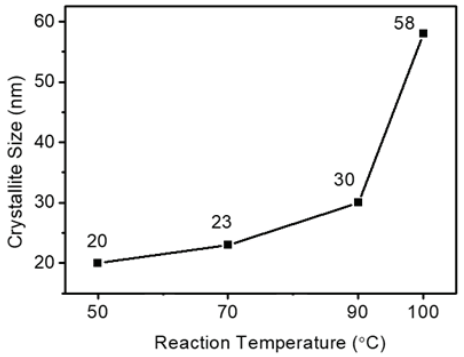

Fig. 6. Variation of crystallite size of Ni-Zn ferrite powders as a function of reaction temperature.

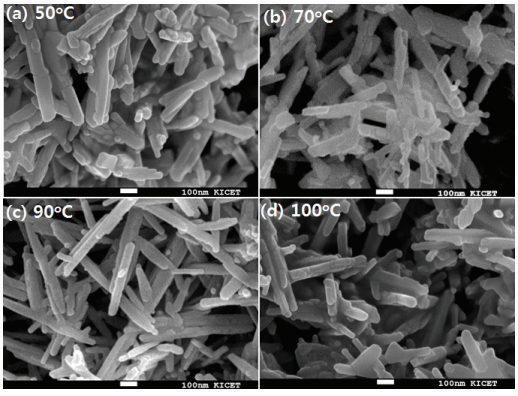

Fig. 7. FE-SEM Image of Ni-Zn ferrite (a) 50℃, (b) 70℃, (c) 90℃, and (d) 100℃.

3.3 Magnetic property

Figure 8 shows the magnetic hysteresis curves (B-H) of Ni-Zn ferrite powders calcined at 700℃ after co-precipitation at four different temperatures.

Figure 9 shows the change in the saturation magnetization (Ms) and the coercive force of the Ni-Zn ferrite powder as a function of the co-precipitation reaction temperature. As the temperature increases from 50℃ to 90℃, the saturation magnetization monotonically increases from 28 emu/g to the maximum saturation magnetization value of 35 emu/g and then drops to the lowest value of 19 emu/g at 100℃ as shown in Fig. 8. It seems to be related to the second phase Fe_2O_3 having a very low saturation magnetization value as compared to the ferrite

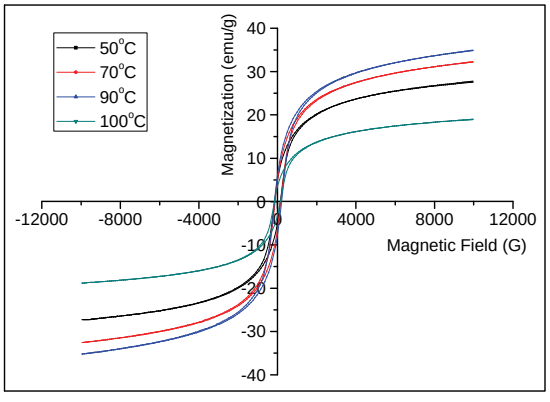

Fig. 8. VSM data of Ni-Zn ferrite (a) 50℃, (b) 70℃, (c) 90℃, and (d) 100℃.

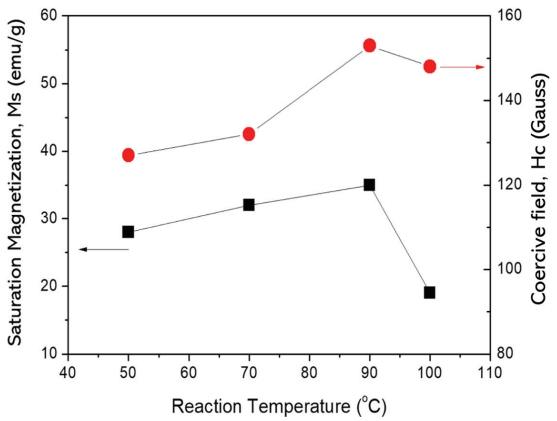

Fig. 9. Ms (emu/g), Hc (Gauss) of Ni-Zn ferrite (a) 50℃, (b) 70℃, (c) 90℃, and (d) 100℃.

observed in the ferrite powder synthesized after co-precipitation at 50 and 100℃ in Fig. 4. It should be noticed that the intensity of α-Fe_2O_3 is further increased at 50 and 100℃. Goethite (α-FeOOH) alone is generally decomposed into Fe_2O_3 as shown in equation (6). Therefore, it seems like that a part of goethite surface did not co-precipitate along with $Zn(OH)_2$ and $Ni(OH)_2$ at 50 and 100℃.

The saturation magnetization (Ms) obtained for our Ni-Zn ferrite powders is lower than the Ms of about 59 emu/g reported for the bulk $Ni_{0.5}Zn_{0.5}Fe_2O_4$ particles [20]. Ms is highly dependent on the change in exchange interactions between tetrahedral and octahedral sites due to crystallinity, particle shape and magnetization direction. In spinel ferrite, the A-B exchange interaction is stronger and more effective than the A-A and B-B exchange interaction [21]. On the other hand, cation distribution and relocation modify the exchange interaction between A and B sites. The deficiency of Zn ions in the tetrahedral A site of the Ni-Zn ferrite can be caused by insufficient co-precipitation of Zn ions in the $Zn(OH)_2$ chemical form, which can move the Fe ions at the B site to the A site and cause a strong A-B exchange interaction to reduce the saturation magnetization [22].

Similarly, as the reaction temperature increases from 50℃ to 100℃, the coercive field (Hc) of the Ni-Zn ferrite powder initially increases from 127 gauss to the highest value of 153 gauss at 90℃ and then it falls to 143 gauss at 100℃.

4. CONCLUSION

Rod-shaped $Ni_{0.5}Zn_{0.5}Fe_2O_4$ particles were successfully synthesized by topotactic reaction method with rod-shaped goethite (FeOOH) particles as main material. The morphology and phase of synthesized NiZn ferrite particles were highly dependent on co-precipitation temperature. Synthesized ferrite particles co-precipitated at 70℃ and 90℃ had a pure spinel structure, but co-precipitated ferrite particles at 50℃ and 100℃ showed secondary phase of Fe_2O_3 in addition to spinel ferrite. The rod-shaped $Ni_{0.5}Zn_{0.5}Fe_2O_4$ particles were best fabricated at a co-precipitation temperature of 90℃, which shows the highest saturation magnetization value of 35 emu/g as well as have nice rod shapes with few debris.

The synthesized Ni-Zn particles co-precipitated in the temperature range of 50 to 90℃ show a monotonic decrease in the lattice parameter but a continuous increase in the saturation magnetization (Ms). This tendency seem to be associated with a higher concentration of Zn ions than that of Ni ions, originated from $Zn(OH)_2$ and $Ni(OH)_2$, in the synthesized particles due to the uneven distribution of constituents caused by the thermal agitation during the co-precipitation process.

REFERENCES

[1] G. R. Amiri, M. H. Yousefi, M. R. Abolhassani, S. Manouchehri, M. H. Keshavarz, and S. Fatahian, *J. Magn. Magn. Mater.*, **323**, 730 (2011). [DOI: https://doi.org/10.1016/j.jmmm.2010.10.034]

[2] Y. Liu, J. J. Li, F. F. Min, J. B. Zhu, and M. X. Zhang, *J. Magn. Magn. Mater.*, **354**, 295 (2014). [DOI: https://doi.org/10.1016/j.jmmm.2013.11.005]

[3] N. Gupta, A. Verma, S. C. Kashyap, and D. C. Dube, *J. Magn. Magn. Mater.*, **308**, 137 (2007). [DOI: https://doi.org/10.1016/j.jmmm.2006.05.015]

[4] K.V.P.M. Shafi, Y. Koltypin, A. Gedanken, R. Prozorov, J. Balogh, J. Lendvai, and I. Felner, *J. Phys. Chem. B*, **101**, 6409 (1997). [DOI: https://doi.org/10.1021/jp970893q]

[5] S. Prasad and N. S. Gajbhiye, *J. Alloys Compd.*, **265**, 87 (1998). [DOI: https://doi.org/10.1016/S0925-8388(97)00431-3]

[6] J. M. Yang, W. J. Tsuo, and F. S. Yen, *J. Solid State Chem.*, **145**, 50 (1999). [DOI: https://doi.org/10.1006/jssc.1999.8215]

[7] Y. Shi, J. Ding, X. Liu, and J. Wang, *J. Magn. Magn. Mater.*,

205, 249 (1999). [DOI: https://doi.org/10.1016/S0304-8853(99)00504-1]

[8] T. F. Marinca, I. Chicinaș, O. Isnard, V. Pop, and F. Popa, *J. Alloys Compd.*, **509**, 7931 (2011). [DOI: https://doi.org/10.1016/j.jallcom.2011.05.040]

[9] D. H. Chen and X. R. He, *Mater. Res. Bull.*, **36**, 1369 (2001). [DOI: https://doi.org/10.1016/S0025-5408(01)00620-1]

[10] H. Kavas, N. Kasapoğlu, A. Baykal, and Y. Köseoğlu, *Chem. Pap.*, **63**, 450 (2009). [DOI: https://doi.org/10.2478/s11696-009-0034-6]

[11] D. P. Volanti, D. Keyson, L. S. Cavalcante, A. Z. Simões, M. R. Joya, E. Longo, J. A. Varela, P. S. Pizani, and A. G. Souza, *J. Alloy. Compd.*, **459**, 537 (2008). [DOI: https://doi.org/10.1016/j.jallcom.2007.05.023]

[12] H. Harzali, F. Saida, A. Marzouki, A. Megriche, F. Baillon, F. Espitalier, and A. Mgaidi, *J. Magn. Magn. Mater.*, **419**, 50 (2016). [DOI: https://doi.org/10.1016/j.jmmm.2016.05.084]

[13] A. M. El-Sayed, *Mater. Chem. Phys.*, **82**, 583 (2003). [DOI: https://doi.org/10.1016/S0254-0584(03)00319-5]

[14] C. Srinivas, B. V. Tirupanyam, S. S. Meena, S. M. Yusuf, C. Seshu Babu, K. S. Ramakrishna, D. M. Potukuchi, and D. L. Sastry, *J. Magn. Magn. Mater.*, **407**, 135 (2016). [DOI: https://doi.org/10.1016/j.jmmm.2016.01.060]

[15] A. T. Raghavender, N. Biliškov, and Ž. Skoko, *Mater. Lett.*, **65**, 677 (2011). [DOI: https://doi.org/10.1016/j.matlet.2010.11.071]

[16] A. P. Kazin, M. N. Rumyantseva, V. E. Prusakov, I. P. Suzdalev, and A. M. Gaskov, *J. Solid State Chem.*, **184**, 2799 (2011). [DOI: https://doi.org/10.1016/j.jssc.2011.08.029]

[17] V. C. Gopalratnam, G. F. Bennett, and R. W. Peters, *J. Environ. Eng.*, **118**, 923 (1992). [DOI: https://doi.org/10.1061/(ASCE)0733-9372(1992)118:6(923)]

[18] K. Velmurugan, V.S.K. Venkatachalapathy, and S. Sendhilnathan, *Mater. Res.*, **13**, 299 (2010). [DOI: https://doi.org/10.1590/S1516-14392010000300005]

[19] C. Srinivas, B. V. Tirupanyam, A. Satish, V. Seshubai, D. L. Sastry, and O. F. Caltun, *J. Magn. Magn. Mater.*, **382**, 15 (2015). [DOI: https://doi.org/10.1016/j.jmmm.2015.01.008]

[20] R. Masrour, H. El Moussaoui, E. Salmani, O. Mounkachi, H. Ez-Zahraouy, M. Hamedoun, E. K. Hlil, and A. Benyoussef, *J. Supercond. Novel Magn.*, **27**, 177 (2014). [DOI: https://doi.org/10.1007/s10948-013-2234-0]

[21] A. Goldman, *Modern Ferrite Technology, 2nd ed.* (Springer, Pittsburgh, 2006) p. 58.

[22] T. Slatineanu, A. R. Iordan, M. N. Palamaru, O. F. Caltun, V. Gafton, and L. Leontie, *Mater. Res. Bull.*, **46**, 1455 (2011). [DOI: https://doi.org/10.1016/j.materresbull.2011.05.002]